Adaptive Maximum Power Point Finding Using Direct $V_{OC}/2$ Tracking Method with Microwatt Power Consumption for Energy Harvesting

Zheng Jun Chew, *Member, IEEE*, and Meiling Zhu, *Member, IEEE*

***Abstract*— Maximum power transfer occurs in many energy harvesters at their half open-circuit voltage ($V_{OC}/2$). A novel implementation method of maximum power point finding based on the $V_{OC}/2$ method is presented by exploiting the capacitor charging voltage across a smoothing capacitor connected in parallel with the energy harvester. The presented technique has a specifically designed high-pass filter which has a peak output voltage that corresponds to the $V_{OC}/2$ of the energy harvester. The control circuit filters and differentiates the voltage across the smoothing capacitor to directly determine the timing of reaching the $V_{OC}/2$ of the energy harvester without having to find the V_{OC} first, and is fully implemented using discrete analog components without the need of a programmable controller, leading to low power consumption of the method. In this paper, the control circuit is used in conjunction with a full wave diode bridge rectifier and a dc–dc converter to harvest energy from a piezoelectric energy harvester (PEH) as the studied case. The PEH was subjected to various strain levels at low frequencies from 2 to 10 Hz. Experimental results show that the implemented circuit is adaptive to various vibration amplitudes and frequencies and has a maximum power point finding efficiency of up to 98.28% with power consumption as low as 5.16 μW.**

***Index Terms*—Adaptive control, analog circuit, energy harvesting, MPPT, piezoelectric devices.**

I. Introduction

ENEERGY harvesting has attracted a lot of attention recently as a potential substitute for batteries in micro to milliwatt power consumption applications such as wireless sensor network where battery replacement is undesirable because of a large number of devices being widely distributed or location inaccessibility. Energy harvesters convert localized ambient energy sources such as light, heat, and vibration into electrical energy. These sources are highly variable depending on the surrounding conditions. Given that the energy required by a sensor node can be relatively constant for a specific application, it is necessary to capture the energy from energy harvesters at their maximum power point (MPP) to ensure that the harvested energy is able to meet the energy demand either immediately or after accumulation of energy within a reasonable timeframe. To date, a few methods that can find the MPP of energy harvesters have been reported, for example, hill-climbing method [1], [2] and fractional open-circuit voltage (FOCV) method [3], [4].

In the hill-climbing method, resistive matching is achieved by dynamically changing the duty cycle of a dc–dc converter in discontinuous conduction mode since it behaves like a variable resistor. Microcontrollers (MCU) [1] or digital circuits [2] are commonly used to repeatedly sense the input voltage and/or current of the energy harvesters to determine the power generated, compare the power generated with a reference, and adjust the duty cycle of the dc–dc converter accordingly to keep track of the MPP. The power required could reach 7.8 mW [1], which is more than the power generated by an energy harvester especially when the availability or intensity of the ambient energy source is low [2], [3]. With the assumption that the environmental change is slow, the duty cycle of the circuit can be kept low by having a short active time and a long sleep time, to reduce the average power consumption to, for example 408 μW [1]. Still, it is probably unsuitable for energy harvesting with micro power because the time to accumulate the energy required for the active operation could be extremely long.

The FOCV method is an a priori method that operates based on the finding that maximum power transfer occurs at certain ratio of the open-circuit voltage V_{OC} of the energy harvesters. This occurs at the half open-circuit voltage $V_{OC}/2$ of energy harvesters such as thermoelectric generators (TEG) [5], and radio frequency rectennas [6], piezoelectric energy harvesters (PEHs) which are generally weakly coupled [7], and around 0.75 to 0.8 V_{OC} for photovoltaic (PV) cells [8]. The circuits which adopted this method can be implemented using full analog discrete component [6] or mixed-signal circuits which involve a sensing capacitor and more subsystems, for example, switch controller [3], or digital controller [4] to perform the FOCV finding algorithms and controls. The energy harvesters are momentarily disconnected from the power management module to obtain their V_{OC}. After that, the energy harvesters can be connected to a voltage divider formed by two resistors to determine the appropriate voltage ratio [6], [8]. The resistor values are properly chosen so that

This work was supported by the Engineering and Physical Sciences Research Council, U.K., through the project En-ComE-Energy Harvesting Powered Wireless Monitoring Systems Based on Integrated Smart Composite Structures and Energy-Aware Architecture under Grant EP/K020331/1. All data are provided in full in the results section of this paper.

Z.J. Chew and M. Zhu are with the College of Engineering, Mathematics and Physical Sciences, University of Exeter, Exeter EX4 4QF U.K. (e-mail: z.j.chew@exeter.ac.uk;m.zhu@exeter.ac.uk).

loading effect on the energy harvester and power consumption is minimized. Alternatively, the V_{OC} is sampled using a sensing capacitor [3], [4]. Then, additional switches and capacitors are used to scale down the sampled V_{OC} to determine the appropriate voltage ratio of the energy harvesters. The power consumption of circuit based on FOCV is usually less than the hill-climbing method, for example, 10 µW in a mixed-signal integrated circuit (IC) [3] and 5.04 µW using full analog discrete components [6]. IC with nanowatts of power consumption has been reported as well, but the input power range is limited between 25 nW and 100 µW [4]. Despite the low power consumption, FOCV may not always be suitable for energy harvester such as PEHs [1], [9], [10] because their V_{OC} is usually high where the voltage can be up to 100 V [10]. Therefore, an actual implementation of the circuit can be expensive and possibly hindered by the voltage limitation of the fabrication technologies [9], [11].

It should be noted that the abovementioned methods can achieve absolute maximum power transfer in energy harvesters which are resistive in nature. However, the power transfer is maximum in relative to those methods for energy harvesters such as PEHs which are intrinsically capacitive [12]. This is because the reactive component introduced by the intrinsic capacitor of PEHs limits the transferable power to less than the maximum power that PEHs can generate [13]. To achieve absolute maximum power, inductive elements are used to complex conjugate the intrinsic capacitance of the PEHs [14]. However, the hill-climbing or FOCV methods are generally easier to implement as a standalone system because complex conjugate matching generally requires an impractically large sized inductor with inductances of hundreds to kilos of Henries [12], [14]. Also, complex conjugate matching is load dependent [12], [14] which still requires a circuit to find the MPP of PEHs. Therefore, this paper focuses on a novel MPP finding method.

This paper herein presents an alternative novel implementation method of $V_{OC}/2$ finding method for energy harvesting without having to find the V_{OC} first. Piezoelectric energy harvesting will be used as the studied case here. The proposed method filters and differentiates the voltage across a capacitor to directly determine the timing of reaching the $V_{OC}/2$ of the PEH by exploiting the RC voltage charging response of the capacitor. This is done using a specifically designed high-pass filter which outputs a peak voltage that corresponds to the $V_{OC}/2$ of the PEH, which is also the voltage when maximum power transfer occurs in that circuit configuration. The presented method is implemented using full analog discrete components with micropower consumption without the needs of programmable controllers or mixed-signal circuits.

II. Proposed Control Method and Analyses

A. Control Method

Fig. 1(a) shows the system architecture for piezoelectric energy harvesting using the novelly implemented analog control circuit in a power management module (PMM). The PEH is connected to a full-wave diode bridge (FB) rectifier for conversion of the ac voltage from the PEH into dc voltage and a smoothing capacitor C_i at the rectifier output to smooth out the rectified voltage. The PMM comprises a dc–dc converter and an analog control circuit which is formed by a high-pass filter, a differentiator, and comparators to realize the novel method of finding $V_{OC}/2$ for a relative maximum power transfer here since the reactance is not cancelled out. The proposed control method is based on the well proven finding that maximum power transfer occurs at $V_{OC}/2$ of the PEH as discussed in the introduction section but uses a novel implementation method by exploiting the voltage charging profile of the smoothing capacitor in conjunction with a specifically designed high-pass filter formed by the capacitor C_{HP} and the resistor R_{HP}, placed in parallel with C_i. The high-pass filter has a peak voltage that corresponds to $V_{OC}/2$ of the PEH if the filter is designed properly as illustrated in Fig. 1 (b). The time that the peak voltage occurs is also the time maximum power transfer occurs in the circuit shown in Fig.

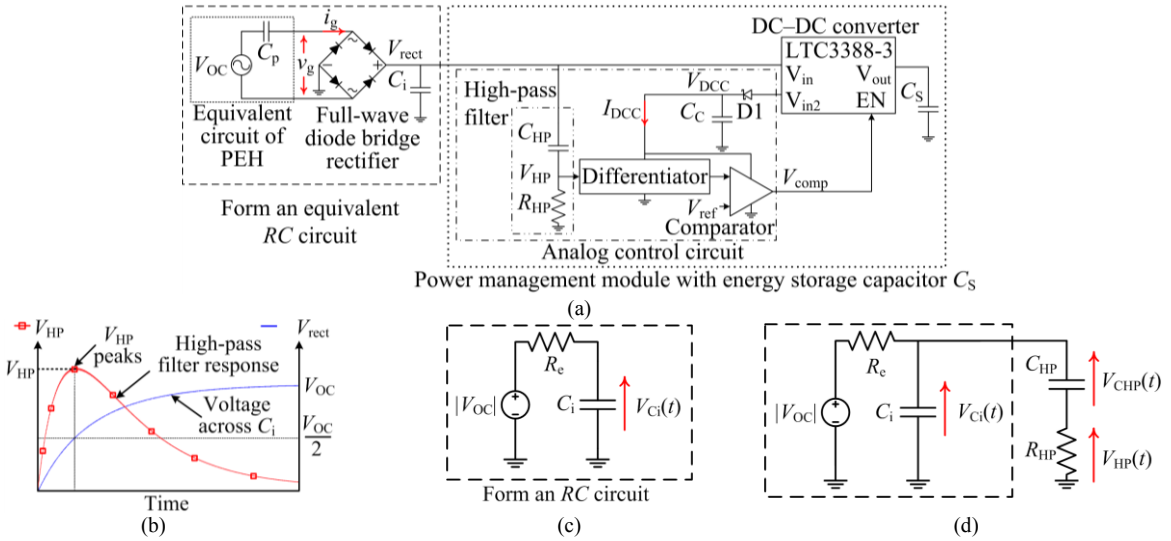

Fig. 1. Schematic of (a) the proposed system architecture for piezoelectric energy harvesting where the PEH, FB rectifier, and smoothing capacitor C_i form an RC circuit, (b) illustrated V_{HP} and V_{rect} showing that V_{HP} peaks at $V_{OC}/2$, (c) circuit model of an equivalent RC circuit formed by an energy harvester represented by $|V_{OC}|$ and R_e in parallel with a capacitor C_i, (d) a high-pass filter is connected in parallel with the smoothing capacitor of the equivalent RC circuit.

1(a). The control circuit then differentiates the output voltage V_{HP} across R_{HP} of the high-pass filter to determine the timing of reaching $V_{OC}/2$ of the PEH without having to find the V_{OC} first. There is no need of a programmable controller where the circuit is fully implemented using discrete analog components.

B. Analyses of $V_{OC}/2$ Finding Method Using RC Circuit

Many energy harvesters exhibit an almost linear *I–V* electrical characteristic and therefore can be modeled as a voltage source with a magnitude of V_{OC} and an equivalent serial resistor R_e [5], [15]. The magnitudes of V_{OC} and R_e mainly correspond to the environmental conditions, for example, temperature difference for TEGs or vibration amplitude and frequency for PEHs. Since most energy harvesters are connected in parallel with a capacitor C_i before a PMM [15], the energy harvester and capacitor can be modeled as an equivalent *RC* circuit as shown in Fig. 1(c), with the PMM ignored first, which reason is given in the last paragraph of Section II.B. The voltage V_{Ci} across the capacitor C_i is given as (1) with the time constant $\tau = R_eC_i$.

$$V_{Ci}(t) = |V_{OC}|\left(1 - e^{-t/\tau}\right) \tag{1}$$

The time t required for V_{Ci} to be charged up to the amplitude which is equal to $|V_{OC}/2|$ is given by (2)

$$t = \tau \ln 2 \tag{2}$$

Therefore, the system is required to detect the timing that $V_{OC}/2$ has reached at $t = \tau\ln2$ for maximum power transfer. An *RC* high-pass filter which is specifically designed in the system, can be used to produce a peak voltage at $t = \tau\ln2$ as the signal to indicate that $V_{OC}/2$ has reached. The analysis is given below.

The *RC* high-pass filter formed by capacitor C_{HP} and resistor R_{HP} in parallel with the equivalent *RC* circuit in Fig. 1(c) is shown in Fig. 1(d). The relationship among the voltages of the loop formed by C_i, C_{HP}, and R_{HP} is given by (3)

$$V_{Ci}(t) = V_{CHP}(t) + V_{HP}(t) \tag{3}$$

Equation (3) can be rewritten as a first order equation as depicted by (4) and solved to obtain (5).

$$V_{Ci}(t) = V_{CHP}(t) + R_{HP}C_{HP}\frac{\mathrm{d}}{\mathrm{d}t}V_{CHP}(t) \tag{4}$$

$$V_{CHP}(t) = V_{Ci}(t)\left(1 - e^{-t/\tau_{HP}}\right) \tag{5}$$

where the time constant τ_{HP} is equal to $R_{HP}C_{HP}$.

Substituting (1) and (5) into (3), V_{HP} can be written as (6).

$$\begin{aligned} V_{HP}(t) &= V_{Ci}(t) - V_{Ci}(t)\left(1 - e^{-t/\tau_{HP}}\right) \\ &= |V_{OC}|\left(e^{-t/\tau_{HP}} - e^{-t\left[1/\tau + 1/\tau_{HP}\right]}\right) \end{aligned} \tag{6}$$

If τ_{HP} is set to be equal to τ, (6) becomes (7)

$$V_{HP}(t) = |V_{OC}|\left(e^{-t/\tau} - e^{-2t/\tau}\right) \tag{7}$$

The time that V_{HP} reaches its peak can be determined by differentiating (7) and solved for t as shown by (8).

$$\begin{aligned} \frac{\mathrm{d}}{\mathrm{d}t}V_{HP}(t) &= |V_{OC}|\left(\frac{2}{\tau}e^{-2t/\tau} - \frac{1}{\tau}e^{-t/\tau}\right) = 0 \\ \frac{1}{\tau}e^{-t/\tau}\left(2e^{-t/\tau} - 1\right) &= 0 \\ t &= \tau \ln 2 \end{aligned} \tag{8}$$

It can be seen that (8) is identical to (2), which means when V_{HP} reaches its peak value, the peak value of V_{HP} is aligned with $V_{OC}/2$ of the PEH, representing that one can use an *RC* circuit to find the maximum power point if τ_{HP} of the filter is properly designed to be equal to τ. Furthermore, from (6), it can be seen that the instant value of V_{HP} is related to the instant V_{Ci} and the amplitude of V_{OC}. From (8), the timing of the peak of V_{HP} is only related to τ when τ_{HP} is set to be τ regardless of the initial value of V_{Ci}. Therefore, the peak of V_{HP} has no relation with the initial V_{Ci} and V_{OC}. For a chosen energy harvester and a chosen value of smoothing capacitor C_i, τ can be known through measurements. This method can be implemented without the need of finding V_{OC} first or using power hungry controllers.

For V_{HP} to peak at a different value of V_{Ci} instead of $V_{OC}/2$ for transducers such as PV cells which have MPP at around $0.75V_{OC}$ [4], (6) should be differentiated with respect to t and solved for τ_{HP} by substituting the t when V_{Ci} reaches the intended fraction of V_{OC} into the first derivative of (6).

In this studied case, the rectified voltage V_{rect} from PEH is equivalent to V_{Ci} in the presented analyses. For ease of analysis, it is assumed that there are no losses in the PEH, the FB rectifier is ideal and C_i is sufficiently large so that V_{rect} presents a smooth dc voltage without ripple. The peak value of V_{rect} equals to $|V_{OC}|$ which corresponds to the vibration applied onto the PEH. V_{rect} exhibits a typical voltage charging profile of a capacitor which will be verified by experiment. Therefore, the rectified PEH and C_i highlighted by the dashed line in Fig. 1(a) can be seen as a dc voltage source with magnitude of V_{OC} and a resistor R_e in series which charges up C_i as shown in Fig. 1(c). The equivalent resistor R_e is related to the impedance of the PEH due to its intrinsic capacitance C_p [15], [16], assuming that the FB rectifier is ideal. The branch formed by C_{HP} and R_{HP} is designed to have an impedance of at least ten times larger than the impedance of the PEH to minimize the loading effect on the PEH so that the branch has negligible effects on V_{rect}.

The dc–dc converter in Fig. 1(a) is initially disabled and is only enabled momentarily to transfer energy from the PEH to the storage capacitor at MPP of the PEH. This applies to other energy harvesters too. The differentiator and comparator have very low current consumption. Therefore, the dc–dc converter, differentiator, and comparator can be regarded as open-circuited and ignored in the circuit analysis. Although the above analyses are based on a constant dc source, the real voltage produced by a PEH is not constant. From (8), it can be seen that the time finding for $V_{OC}/2$ is independent of V_{OC}. Therefore, this method can be suitable for varying voltage, which will be verified experimentally in Section V. In addition, it should be noted that the purpose of the simplified theoretical analyses presented here is to aid the reader to

understand that $V_{OC}/2$ can be found using the high-pass filter and differentiator if the filter is designed properly at the condition of $\tau_{HP} = \tau$, and it is not for finding the parameters of the high-pass filter. The design of the filter will be discussed in Section III.B for a chosen PEH with a chosen range of operational frequency.

III. System Implementation and Operation

Schematic of the proposed system and the detailed implementation of the analog control circuit are shown in Figs. 1(a) and 2 respectively. The FB rectifier is composed of four BAS70 Schottky diodes which have low forward voltage drop and low leakage current so that the power loss is low. The dc–dc converter chosen is a buck converter (DC1658A-B, demo board of LTC3388-3) to step down the voltage produced by a PEH because the produced voltage is usually higher than the voltage usable by low power electronic devices such as wireless sensor nodes which have an operating voltage range of 1.8–3.8 V [17]. A supercapacitor is used for energy storage.

A. Power Source of Analog Control Circuit

The power source of the analog control circuit is taken from an internal rail V_{in2} of the buck converter as shown in Fig. 1(a) for implementation simplicity to avoid introducing an extra circuit for a lower regulated voltage supply and extra power consumption associated with that circuit in the proposed analog control circuit. V_{in2} can provide a regulated voltage at 4.6 V from the input voltage V_{rect} fed into the buck converter even when the buck converter is disabled. This means the proposed system can self-start without any issue by using the input power directly from the PEH unless the voltage generated by the PEH is extremely low, below the operating voltages of the components used due to extremely low vibration. The voltage from V_{in2} is equal to V_{rect} before it reaches 4.6 V but will be steady at 4.6 V if V_{rect} is higher than 4.6 V. Therefore, V_{in2} will fluctuate with V_{rect} when its amplitude is low. To ensure that the supply voltage given to the analog control circuit is stable, diode D1 (BAS70) and capacitor C_C are used. Taking the forward diode drop of D1 into account, capacitor C_C holds the supply voltage at around 4.3 V. Diode D1 prevents the current from flowing back into the buck converter when V_{rect} drops below 4.3 V. Therefore, V_{DCC} can stay relatively stable even when there is a sudden drop in the voltage provided by the internal rail of the buck converter.

B. Implementation of High-pass Filter and Differentiator

The buck converter is disabled initially, and can be regarded as open-circuited which allows the PEH, FB rectifier, and smoothing capacitor to effectively form an equivalent *RC* circuit as discussed earlier. From Fig. 2, C_{HP}, R1, and R2 form the high-pass filter, where voltage across R1 and R2 is V_{HP}. V_{HP} is taken as the input to the differentiator realized by a nano-current operational amplifier (LPV521MGE). Output from the differentiator V_{diff} is passed through an envelope detector for a smoother signal as V_{ED}, which is used to compare with a reference voltage V_{ref} by the comparator Comp 1 (TS881ICT). In theory, the differentiation of a peak value is equal to zero for the timing of maximum power transfer. However, in practice, it is difficult for a comparator to compare a zero value with a reference which is zero as well where the output could be unpredictable. Therefore, V_{ref} implemented in the circuit is slightly away from zero and is designed in such a way in the circuit that V_{ref} comes from V_{RD} which is a scaled down voltage from V_{rect} using the voltage divider formed by R_{D1} and R_{D2}, and then by passing V_{RD} through a diode D2 (1N754A). This implementation method is viable because the power that can be transferred with slight deviation from $V_{OC}/2$ is still close to the power available at the MPP of the PEH, which will be verified in Section V.

To best design the filter with τ_{HP} equals τ, the time constant τ of the equivalent *RC* circuit formed by the chosen PEH, FB rectifier, and C_i as shown in Fig. 1(c) was measured at 6 Hz in this paper. With τ known from the measurement, many combinations of resistances and capacitances can lead to the same τ_{HP}. To minimize the amount of power dissipated by the resistors and the loading effect on the smoothing capacitor C_i, the total resistance of R1 and R2 are chosen as 20 MΩ and then the value of C_{HP} is determined accordingly. For other types of energy harvesters or operational ranges, the values of C_i, C_{HP}, R1, and R2 can be tuned in a similar way to suit the application.

C. DC–DC Converter for Power Transfer Operation

Another comparator Comp 2 (LTC1540) is used to enable or disable the buck converter. Comp 2 has an internal bandgap reference voltage which is always higher than the amplitude of V_{RD}. The bandgap reference voltage is fed to the inverting input while V_{RD} is fed to the non-inverting input of Comp 2 so that V_{comp} generated is LOW to disable the buck converter for most of the time before V_{HP} reaches its peak.

When V_{HP} reaches its peak, V_{CSH} which is held by a sample and hold (S/H) circuit formed by Comp 1, MOSFET M_{SH} (FDC6420C), and C_{SH} is fed to the inverting input of Comp 2 while V_{RD} at the non-inverting input of Comp 2 continue to rise. Subsequently, V_{comp} becomes HIGH, which starts the

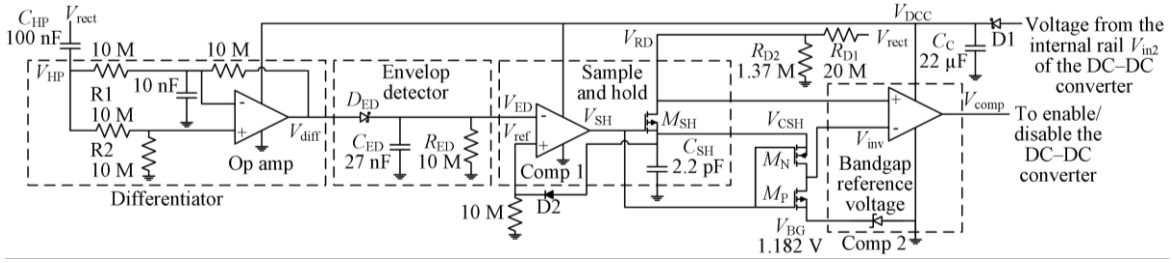

Fig. 2. Schematic of detailed implementation of the analog control circuit.

buck converter to transfer power from the PEH to the storage capacitor C_S until V_{RD} drops below V_{CSH}. V_{rect} will drop below $V_{OC}/2$ at the end of the power transfer and causes a drop in V_{HP}, which disables the buck converter at the end of this cycle. This allows V_{rect} to rise again towards $V_{OC}/2$ and the cycle repeats with the next search for V_{HP} reaching its peak.

IV. Experimental and Evaluation Methods

The experiments were conducted with two different circuit configurations to verify the performance of the proposed method for maximum power transfer in piezoelectric energy harvesting. The first configuration (CFG 1) used is the implemented system as shown in Fig. 1(a) where the PEH is connected with a power management module (PMM) with the proposed analog control circuit after the FB rectifier. In CFG 2, the PMM and energy storage highlighted in the dotted line is replaced by a variable resistor, placed in parallel with a capacitor to measure the maximum power that can be generated by the PEH interfaced with a FB rectifier for comparison purpose. The optimal resistive load for CFG 2 is determined by manually tuning the variable resistor until maximum power generated by the PEH is found. CFG 2 is used because in most circuit designs [1], [9], [10], a smoothing capacitor is always required after the rectifier to smooth out the rectified voltage, which is similar to the implemented system for fair comparison. The value of C_i used in CFG 1 and CFG 2 is the same 22 µF and is chosen so that C_i is much larger than the intrinsic capacitance C_P of around 200 nF of the PEH for a more efficient power transfer [10]. Signals in the analog control circuit were also measured to verify the circuit operation. The circuit was built on a breadboard for ease of measurement.

A. Testbed Setup

A M8528-P2 macro-fiber composite (MFC) piezoelectric transducer bonded on a composite material using epoxy was used as the PEH [14], as illustrated in Fig. 3. Both ends of the MFC PEH was held firmly in an Instron E10000 ElectroPuls dynamic and fatigue test machine by its two grips where one is movable and one is fixed as shown in Fig. 3. The movable grip applies different strain and frequency loadings onto the composite substrate by its upwards and downwards movement. With such a cyclic loading applied onto the composite substrate, the PEH generates a sinusoidal output.

B. Input Vibration

It is important to verify that the implemented circuit is adaptive to the variation of vibrational conditions in an ambient environment for actual deployment in real-world applications. For this test, a sweep test at 10 Hz using peak-to-peak strain loadings from 300 µε to 500 µε, and then back to 300 µε was applied onto the PEH. Tests of applying different frequencies from 2 to 10 Hz and different mechanical loadings with peak-to-peak strain levels of 300 µε, 400 µε, and 500 µε using the Instron machine were also carried out on both circuit CFGs 1 and 2, where the power generated by the PEH is measured.

C. Measurements and Calculations

Fig. 3 shows the measurement setup for performance verification. A National Instrument (NI) data acquisition system (DAQ) was used to measure the voltage v_g generated by the PEH in CFG 2 for finding the maximum power which can be generated while tuning the variable resistor to its optimal value since the NI DAQ can show real-time measurement results. Keithley 2612B sourcemeter units (SMUs) which have a higher resolution than NI DAQ were then used to measure v_g and i_g generated by the PEH for both circuit CFG 1 and CFG 2.

The instantaneous power p_g generated by the PEH is the product of v_g and i_g as given by (9). The time average of (9) is the average power produced by the PEH as depicted by (10).

$$p_g(t) = v_g(t) i_g(t) \tag{9}$$

$$P_g = \frac{1}{T}\int_0^T p_g(t)\,\mathrm{d}t \tag{10}$$

To distinguish the power generated by the PEH in circuit CFG 1 and CFG 2, the subscripts 'PMM' and 'rc' which represent the two different circuit configurations which were connected at the rectifier output will be added. Voltages V_{rect}, V_{DCC}, and current I_{DCC} of circuit CFG 1 were also measured using the SMUs. The power P_{RD} dissipated by the resistors R_{D1} and R_{D2} was calculated using (11) and the power P_{DCC} consumed by the control circuit formed by the differentiator and comparators as shown in Fig. 2 was determined by (12).

$$P_{RD} = \frac{\sum_{k=1}^{N} V_{rect}^{\ 2}(t_k)\Delta t}{t(N)(R_{D1}+R_{D2})} \tag{11}$$

$$P_{DCC} = \frac{\sum_{k=1}^{N} V_{DCC}(t_k) I_{DCC}(t_k)\Delta t}{t(N)} \tag{12}$$

where Δt is the sampling time of the SMUs and $t(N)$ is the

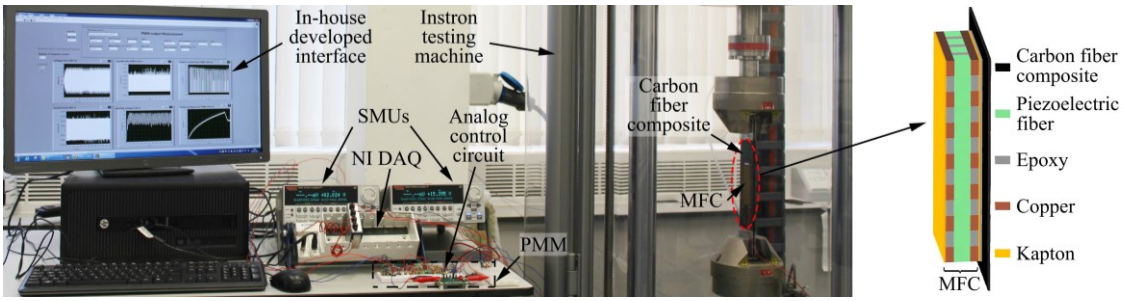

Fig. 3. Image of the experimental setup and illustration of the mechanical structure of the PEH.

time taken to do the measurement. The NI DAQ system and SMUs were connected to a computer and controlled via a LabVIEW interface to record all the measurements into the computer.

D. Metrics for Efficiency

$P_{\text{g-rc}}$ which is the maximum power generated by the PEH in CFG 2 with an optimal load will be used as a reference to assess the capability of maximum power transfer from CFG 1 with the proposed method, that is, if the power generated $P_{\text{g-PMM}}$ from the implemented circuit CFG 1 can match $P_{\text{g-rc}}$ in percentage. Therefore, the capability for maximum power transfer from the PEH using circuit CFG 1 η_{MPT} is defined as the ratio of $P_{\text{g-PMM}}$ to $P_{\text{g-rc}}$ as given by (13).

$$\eta_{\text{MPT}} = \frac{P_{\text{g-PMM}}}{P_{\text{g-rc}}} \times 100\% \tag{13}$$

The total power consumption P_{ACC} of the analog control circuit is the summation of (11) and (12) as given by (14).

$$P_{\text{ACC}} = P_{\text{RD}} + P_{\text{DCC}} \tag{14}$$

V. Results and Discussions

A. $V_{OC}/2$ Finding

To show that V_{HP} will indeed reach its peak at $V_{\text{OC}}/2$ of a PEH, the buck converter was deliberately disabled all the time when the PEH was subjected to a peak-to-peak strain loading of 300 με at 6 Hz as an example while V_{rect} and V_{HP} were measured using an oscilloscope with the results shown in Fig. 4. V_{rect} shows a typical capacitor charging profile, which validates the circuit model used in Section II.B for the theoretical analyses.

Still using the strain loading of 300 με at 6 Hz as an example, Fig. 5 shows the measured V_{rect}, V_{HP}, V_{diff}, V_{ED}, V_{ref}, and V_{comp} to verify the normal operation of the implemented analog control circuit in enabling the buck converter for power transfer from the PEH to the energy storage. It can be seen that the analog control circuit can closely finds $V_{\text{OC}}/2$ of the PEH when V_{HP} reaches its peak for that test condition. V_{comp} becomes HIGH to enable the buck converter to transfer energy to the energy storage, and hence V_{rect} starts to drop. V_{ref} has some pulses after the V_{HP} peaks due to the fluctuations at V_{ref} caused by the power transfer but they have no effect on the power transfer after V_{HP} peaks because once the power transfer begins, it continues until V_{rect} drops to a certain level instead of transferring once at a fixed point. When V_{rect} drops to a certain level after the power transfer, V_{comp} becomes completely LOW again to disable the buck converter and the whole cycle repeats. The V_{HP} shown in Fig. 5 has some ripple because all the components are now under normal operation, drawing more current than the circuit which produces the V_{HP} shown in Fig. 4. The ripple causes V_{diff} to become a pulse-like output with decreasing magnitude as V_{HP} is approaching its peak. The envelope detector effectively converts V_{diff} into V_{ED} to avoid false detection of the peak of V_{HP} since V_{diff} goes to zero multiple times.

B. Maximum Power Transfer Efficiency

In this paper, the vibration frequency range of interest is 2 to 10 Hz. Therefore, the high-pass filter was designed to have

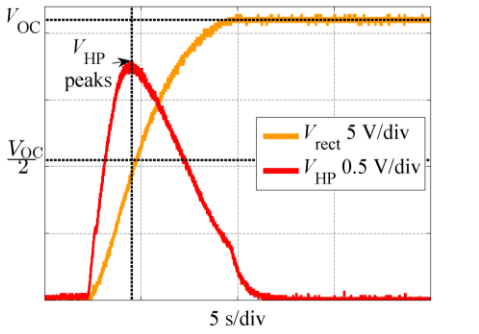

Fig. 4. V_{HP} peaks at V_{rect} equals to $V_{\text{OC}}/2$ with the buck converter disabled when the PEH is subjected to peak-to-peak strain loading of 300 με at 6 Hz.

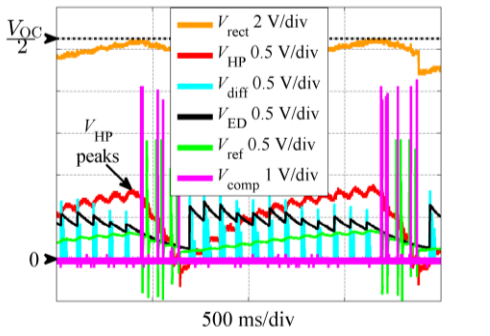

Fig. 5. Measured V_{rect}, V_{HP}, V_{diff}, V_{ED}, V_{ref}, and V_{comp} to show the operation of the implemented analog control circuit in enabling the buck converter for power transfer when the PEH is subjected to a peak-to-peak strain loading of 300 με at 6 Hz.

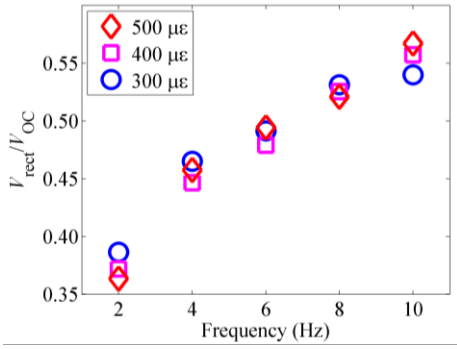

Fig. 6. Ratio of V_{rect} to V_{OC} at different strain levels and frequencies showing that energy can be harvested away from $V_{\text{OC}}/2$.

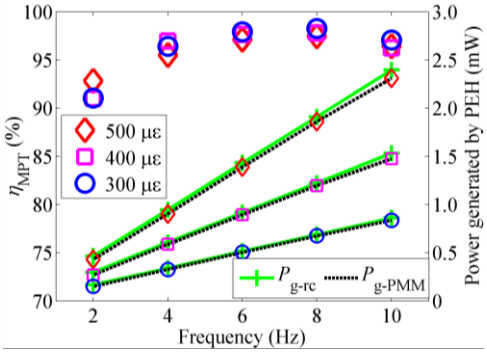

Fig. 7. η_{MPT} of the proposed circuit obtained by comparing the power generated by the PEH using circuit CFG 1, $P_{\text{g-PMM}}$ (dash) with the power generated by the PEH using circuit CFG 2, $P_{\text{g-rc}}$ (solid) at different frequencies and strain levels of 300 με (○), 400 με (□), and 500 με (◊).

V_{HP} peaks at $V_{OC}/2$ for the frequency of 6 Hz, which is at the center of the frequency range of interest so that the power harvested at the other frequencies is near to the maximum power that can be transferred from the PEH in this circuit configuration.

As discussed above, the proposed circuit can closely find $V_{OC}/2$ at one specifically designed vibration frequency but has lower accuracies for other vibration frequencies because the time V_{HP} peaks is mainly determined by the specifically designed high-pass filter with a fixed time constant in this implemented circuit. Therefore, the time where V_{HP} reaches its peak at $V_{OC}/2$ only occurs at around 6 Hz for the implemented circuit as shown in Figs. 4 and 5. The ratio of V_{rect} to V_{OC} at different strain levels and frequencies are shown in Fig. 6. It can be seen that the implemented circuit initiates power transfer at approximately $V_{OC}/2$ with accuracy of 72 to 99 % for the tested frequencies and strain loadings. The question raised here is when the derivative of V_{HP} equals zero is away from $V_{OC}/2$, how much of the power harvested is away from the power available at MPP of the PEH?

Fig. 7 compares $P_{g\text{-}PMM}$ with $P_{g\text{-}rc}$ that is generated by the PEH subjected to different strain loadings and frequencies. The results show that $P_{g\text{-}PMM}$ ranges from 152 µW to 2.3 mW and is very close to $P_{g\text{-}rc}$ for all the tests. This means the implemented circuit can be powered directly by using the input power from the PEH and is able to harvest energy from the PEH with η_{MPT} of 91.07 to 98.28 %, calculated using (13) for all the tests. With the efficiency staying above 90 %, the energy harvesting capability of the implemented circuit is high. The trend of η_{MPT} agrees with the results shown in Fig. 6, where the efficiency is the lowest at 2 Hz and gradually increases as the frequency increases. Peak efficiency is around 6 and 8 Hz before it drops again at 10 Hz. It can be concluded that $V_{OC}/2$ based method have high tolerance of harvesting energy at the voltage away from $V_{OC}/2$. This can also be explained using the obtained experimental power curves that change with respect to voltages from CFG 2, as shown in Fig. 8, while the variable resister is being tuned to find the MPP of the PEH. The power curve is parabolic, meaning that the power deviates a little from its MPP although the voltage is away from $V_{OC}/2$ at higher percentages. For example, even though the voltage of the implemented method is away by ±30 % from $V_{OC}/2$, which is at 0.7 or 1.3$V_{OC}/2$, 91 % of the power available at MPP can still be obtained and the trend remains the same regardless of the changes in frequency or V_{OC}. It should be noted that the studied case in this paper is one of the worst cases as the impedance $|2\pi fC_p|^{-1}$ of the PEH changes drastically at low frequencies and gently decreases at higher frequencies like an exponential decay. With the time constant $\tau = R_eC_i$ and C_i is fixed, τ against frequency will therefore show a similar profile as $|2\pi fC_p|^{-1}$ which is the main element contributing towards R_e. The proposed method shows good performance at low frequencies and is expected to work well at higher frequencies over a wide range of frequencies based on theoretical changes of τ with R_e if the filter is designed for a high operational frequency.

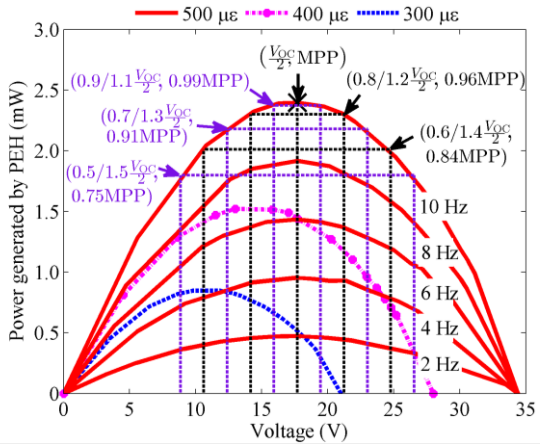

Fig. 8. Matter of accuracy in finding MPP based on $V_{OC}/2$ method by using strain loading of 500 με (solid) at different frequencies as example. Power curves for strain loadings of 300 με (dash) and 400 με (dash-dot) at 10 Hz are also plotted to show that the method works for different V_{OC}.

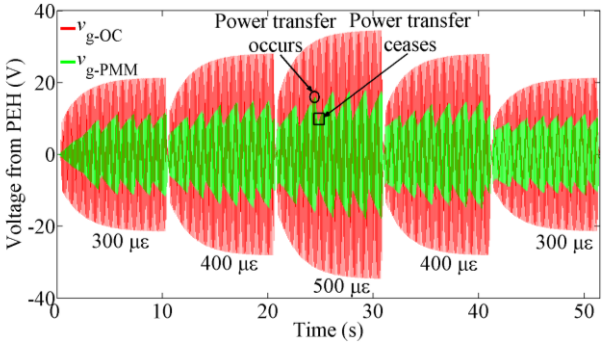

Fig. 9. Measured $v_{g\text{-}OC}$ (higher amplitude) and $v_{g\text{-}PMM}$ generated by the PEH when it is open-circuited and connected to the power management module respectively in a sweep test. Peak voltage of $v_{g\text{-}PMM}$ is around $V_{OC}/2$ when power transfer occurs, as pointed at one of the occurrences circled in the figure.

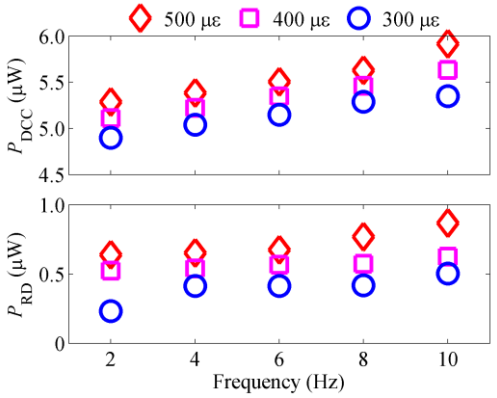

Fig. 10. Power consumption P_{DCC} of the differentiator and comparators in the implemented control circuit (top) and the power P_{RD} dissipated by R_{D1} and R_{D2} (bottom) at different frequencies and strain levels.

C. *Adaptability*

Results from Fig. 7 prove that the implemented circuit is adaptive to the changes of input vibration as it can harvest energy from the PEH with high efficiency under different test conditions. The sweep test from 300 με to 500 με and back to 300 με at 10 Hz further proves that the circuit is adaptive to real time changes as shown in Fig. 9. The PEH which was in open-circuit produced different open-circuit voltages $v_{g\text{-}OC}$

when it experienced different strain levels. A circuit which is adaptive has to be able to initiate the power transfer process at different voltage levels when the PEH is subjected to different strain levels. Measured $v_{g\text{-}PMM}$ from the sweep test shows that the implemented analog control circuit can indeed initiate the power transfer process at different voltage levels. This proves that the implemented circuit is able to respond to real-time changes of a vibration source.

Using one of the occurrences at 500 με as example, the sawtooth-like waveform of $v_{g\text{-}PMM}$ can be explained as follows. The circuit initiates the power transfer at around $V_{OC}/2$ as circled in Fig. 9. The power transfer process causes the voltage $v_{g\text{-}PMM}$ from the PEH to drop, and thus the circuit ceases the power transfer after the voltage drops as indicated by the square symbol in Fig. 9 because it moves away from the $V_{OC}/2$. This allows the voltage from the PEH to rise back to the value of around $V_{OC}/2$ and the whole power transfer process cycle repeats as long as there is a vibration exciting the PEH.

It should be noted that the Instron machine requires some time to reach its steady state operation. Therefore, the voltage waveform gradually increases whenever there is a change of strain loading applied onto the composite substrate. From the results shown in Fig. 9, the circuit initiates power transfer at about $V_{OC}/2$ of the PEH even though the vibration exerted onto the PEH is not at its steady state yet. Therefore, it can be further justified that the implemented method is suitable for a time-varying amplitude vibration which usually happens in the real-world rather than just a constant amplitude vibration.

It should also be noted that amplitude of the voltage produced by the PEH changes with the vibration applied and V_{rect} changes accordingly too. The implemented circuit is able to adapt to the changes since many parts of the circuit such as the high-pass filter and the differentiator as well as parameters such as V_{RD}, V_{CSH}, and V_{ref} changes with V_{rect}.

D. Power Consumptions

The power consumptions P_{DCC} and P_{RD} of the analog control circuit as shown in Fig. 2 are given in Fig. 10. It can be seen that P_{DCC} slightly increases with both the strain levels and the frequencies applied on the PEH. Equation (11) shows that the power P_{RD} dissipated at the resistive divider network is related to V_{rect}. When the PEH experiences a higher strain level, V_{rect} will become higher because of a higher voltage, $v_{g\text{-}PMM}$, produced by the PEH, as shown in Fig. 9. The circuit will therefore harvest the energy at a higher $v_{g\text{-}PMM}$ and with the higher V_{rect}, dissipate more power according to (11).

Fig. 10 indicates that the power consumption of the implemented circuit increases with frequency. This is because with higher vibration frequency applied onto the PEH as shown in Fig. 8, more power can be generated, and thus V_{rect} can be charged up quicker and more often to $V_{OC}/2$ in a given period of time. The analog control circuit has to operate more frequently to initiate the power transfer in response to the changes of V_{rect}, and thus consumes more power. Fig. 11 shows the current I_{DCC} consumed by the analog control circuit with the applied peak-to-peak strain loadings of 300 με at 2 Hz and 10 Hz onto the PEH as examples. The analog control circuit can be seen to operate more often as more current peaks are seen when a higher frequency is applied onto the PEH. The initial inrush current is also higher at 10 Hz because there is more power generated by the PEH at a higher frequency, which leads to a higher average current consumption. V_{DCC} of the analog control circuit shown in Fig. 11 further confirms the low current consumption of the circuit since V_{DCC} does not drop when the analog control circuit is operating. This also indicates that stable voltage can be supplied to the circuit using D1 and C_C.

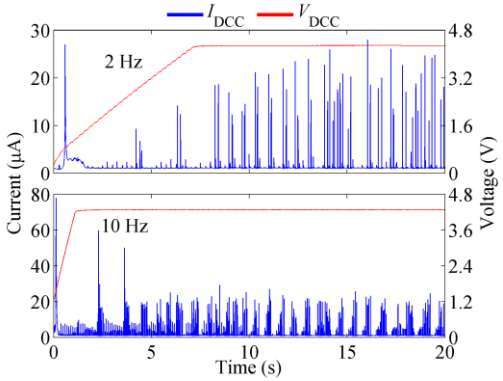

Fig. 11. Current I_{DCC} and voltage V_{DCC} measured when the PEH is subjected to a strain level of 300 με at 2 Hz (top) and 10 Hz (bottom).

The measured power consumption P_{ACC} of the proposed circuit implemented using discrete components in the studied case is between 5.16 μW and 6.78 μW, which is comparable to the design using discrete components with power consumption of 5.04 μW in [6]. Such a low power consumption enables the circuit to be powered up entirely using the input power from the energy harvesters, which significantly reduces the risk of start-up issue and does not require a start-up circuit.

VI. Conclusion

An adaptive microwatt power consumption analog control circuit that employs a novel $V_{OC}/2$ finding scheme by exploiting the *RC* response of a charging capacitor voltage profile and introducing a specifically designed high-pass filter with a peak voltage that corresponds to the $V_{OC}/2$ is presented here. The control circuit filters and differentiates the voltage across a capacitor to directly determine the timing of reaching the $V_{OC}/2$ of an energy harvester. The method was demonstrated to harvest energy from an MFC piezoelectric transducer which was subjected to various vibrational frequencies and strain loadings as an example. The proposed method for maximum power transfer from the PEH based on the rectified voltage across the smoothing capacitor is shown to have a high tolerance of harvesting energy at the voltage away from $V_{OC}/2$. More than 90 % of the maximum power available can still be harvested even when the voltage is away from $V_{OC}/2$ by up to ±30 %. The implemented power management module with the proposed control circuit is able to harvest as much as 98.28 % of the power that the PEH can generate when it was connected with its optimal resistive load. The circuit is also adaptive to real-time amplitude changes as

demonstrated in the strain level sweep test.

The control circuit is fully implemented using low power analog discrete components without the need of more than one capacitor-switch pair and other associated subsystems as required in many reported mixed-signal circuits which determine $V_{OC}/2$ via charge sharing. This circuit consumes between 5.16 μW and 6.78 μW of power for all the tested conditions, which is around 7 to 872 times lower than the controllers for hill-climbing method and comparable with other reported FOCV circuits. In addition to its low power consumption, performance of the circuit is not compromised where the peak maximum power transfer efficiency is up to 98.28 %. This low power feature is crucial especially in the case of PEHs working at off-resonance because the power which can be harvested is much lower than those in resonance. This allows the proposed circuit to be powered up directly by the PEHs.

Since the circuit is fully implemented using analog discrete components, the proposed circuit can be easily fabricated as a monolithic IC. It is worthwhile to mention that, although the proposed method and circuit topology are evaluated using a PEH under different strain loadings within a frequency range of interest to achieve a relative maximum power transfer in this paper, the strain loading was actually generated by a controlled force setting in the Instron machine. Therefore, the proposed circuit is suitable for general PEHs under a force excitation at their base to achieve a relative maximum power transfer within a frequency range of interest. From the theoretical analysis, the proposed method is also suitable for other energy harvesters that can be modeled as a dc voltage source with an equivalent series resistance to achieve an absolute maximum power transfer. The circuit may also be combined with SSHI technique for increased energy harvesting from PEHs. With the lower power requirement and reduced size of an IC, this circuit can potentially be suitable for a wide range of applications in real-world situations for low power energy harvesting based devices owing to its low power consumption, tolerance to frequency changes, adaptiveness to amplitude changes, and versatility to different types of energy harvesters.

REFERENCES

[1] N. Kong, and D.-S. Ha, "Low-power design of a self-powered piezoelectric energy harvesting system with maximum power point tracking," *IEEE Trans. Power Electron.,* vol. 27, no. 5, pp. 2298-2308, 2012.

[2] H. Kim, S. Kim, C. K. Kwon, Y. J. Min, C. Kim, and S. W. Kim, "An energy-efficient fast maximum power point tracking circuit in an 800-μW photovoltaic energy harvester," *IEEE Trans. Power Electron.,* vol. 28, no. 6, pp. 2927-2935, 2013.

[3] M. Shim, J. Kim, J. Jeong, S. Park, and C. Kim, "Self-powered 30 μW to 10 mW piezoelectric energy harvesting system with 9.09 ms/V maximum power point tracking time," *IEEE J. Solid-State Circuits,* vol. 50, no. 10, pp. 2367-2379, 2015.

[4] G. Chowdary, A. Singh, and S. Chatterjee, "An 18 nA, 87% efficient solar, vibration and RF energy-harvesting power management system with a single shared inductor," *IEEE J. Solid-State Circuits,* vol. 51, no. 10, pp. 2501-2513, 2016.

[5] A. Montecucco, and A. R. Knox, "Maximum power point tracking converter based on the open-circuit voltage method for thermoelectric generators," *IEEE Trans. Power Electron.,* vol. 30, no. 2, pp. 828-839, 2015.

[6] D. Masotti, A. Costanzo, P. Francia, M. Filippi, and A. Romani, "A load-modulated rectifier for RF micropower harvesting with start-up strategies," *IEEE Trans. Microw. Theory Tech.,* vol. 62, no. 4, pp. 994-1004, 2014.

[7] Y. C. Shu, I. C. Lien, and W. J. Wu, "An improved analysis of the SSHI interface in piezoelectric energy harvesting," *Smart Mater. Struct.,* vol. 16, no. 6, pp. 2253-2264, 2007.

[8] A. S. Weddell, G. V. Merrett, and B. M. Al-Hashimi, "Photovoltaic sample-and-hold circuit enabling MPPT indoors for low-power systems," *IEEE Trans. Circuits Syst. I, Reg. Papers,* vol. 59, no. 6, pp. 1196-1204, 2012.

[9] A. Tabesh, and L. G. Fréchette, "A low-power stand-alone adaptive circuit for harvesting energy from a piezoelectric micropower generator," *IEEE Trans. Ind. Electron.,* vol. 57, no. 3, pp. 840-849, 2010.

[10] G. K. Ottman, H. F. Hofmann, A. C. Bhatt, and G. A. Lesieutre, "Adaptive piezoelectric energy harvesting circuit for wireless remote power supply," *IEEE Trans. Power Electron.,* vol. 17, no. 5, pp. 669-676, 2002.

[11] P. Gasnier, J. Willemin, S. Boisseau, G. Despesse, C. Condemine, G. Gouvernet, and J. J. Chaillout, "An autonomous piezoelectric energy harvesting IC based on a synchronous multi-shot technique," *IEEE J. Solid-State Circuits,* vol. 49, no. 7, pp. 1561-1570, 2014.

[12] N. Kong, D. S. Ha, A. Erturk, and D. J. Inman, "Resistive impedance matching circuit for piezoelectric energy harvesting," *J. Intell. Mater. Syst. Struct.,* vol. 10, no. 13, pp. 1293-1302, Jan., 2010.

[13] Y. K. Ramadass, and A. P. Chandrakasan, "An efficient piezoelectric energy harvesting interface circuit using a bias-flip rectifier and shared inductor," *IEEE J. Solid-State Circuits,* vol. 45, no. 1, pp. 189-204, 2010.

[14] A. Giuliano, and M. Zhu, "A passive impedance matching interface using a PC permalloy coil for practically enhanced piezoelectric energy harvester performance at low frequency," *IEEE Sensors J.,* vol. 14, no. 8, pp. 2773-2781, 2014.

[15] S. Bandyopadhyay, and A. P. Chandrakasan, "Platform architecture for solar, thermal, and vibration energy combining with MPPT and single inductor," *IEEE J. Solid-State Circuits,* vol. 47, no. 9, pp. 2199-2215, 2012.

[16] H. Xia, R. Chen, L. Ren, and Q. Zhou, "Direct calculation of source impedance to adaptive maximum power point tracking for broadband vibration energy harvesting," *J. Intell. Mater. Syst. Struct.,* vol. 28, no. 9, pp. 1105-1114, 2017.

[17] E. Casilari, J. M. Cano-García, and G. Campos-Garrido, "Modeling of current consumption in 802.15.4/ZigBee sensor motes," *Sensors,* vol. 10, no. 6, pp. 5443-5468, 2010.